Effects of Size, Composition, and Architecture on the CO Tolerance of Bimetallic Co_xPt_y Nanoparticle Electrocatalysts

C. M. Sims and B. W. Eichhorn

Department of Chemistry and Biochemistry
University of Maryland, College Park
College Park, MD, USA, eichhorn@umd.edu

ABSTRACT

$CoPt_3$, CoPt, and Co_3Pt (Co_xPt_y) alloy and intermetallic nanoparticle (NP) electrocatalysts were synthesized and characterized by a combination of powder X-ray diffraction (XRD), transmission electron microscopy (TEM), and energy dispersive spectroscopy (EDS) studies. Electrochemical carbon monoxide (CO) stripping and rotating disk electrochemical (RDE) experiments showed that the Co_xPt_y alloy NPs have CO-tolerant hydrogen oxidation reaction (HOR) performances similar to monometallic Pt catalysts, but the structural and electronic modifications induced by intermetallic formation were found to be detrimental to their ability to tolerate CO. However, the decreased Pt content makes them more cost-effective as electrocatalysts for proton exchange membrane fuel cells (PEMFCs).

Keywords: bimetallic nanoparticles, electrocatalysis, fuel cells, heterogenous catalysis, intermetallics

1 INTRODUCTION

PEMFCs are highly regarded as a clean alternative energy technology for motor vehicles, power generators, and many other applications. Unfortunately, several factors limit their commercial viability, including the high expense of their catalytic materials, the poisoning of the HOR electrocatalyst at the anode by CO, and the inefficiency of the oxygen reduction reaction (ORR) electrocatalyst at the cathode. To mitigate these issues, researchers have developed new Pt-based bimetallic nanoparticles (NPs) by alloying Pt with cheaper metals such as Fe,[1] or Cu.[2] Use of these bimetallic NPs has led to reduced catalyst costs, improved CO tolerance for the HOR, and increased catalytic efficiencies for the ORR.

Although the Co-Pt bimetallic system has been extensively studied for ORR catalysis, with high catalytic activities predicted by theoretical models and demonstrated in the literature,[3-8] research into the use of Co-Pt NPs for CO-tolerant HOR catalysis is quite limited.[9,10] While these previous studies reported mild improvements in CO tolerance from Co-alloying, the Pt-rich $CoPt_3$ alloy was the focus of research,[9,10] with little discussion of other compositions or architectures.[9] In our previous work, the CO tolerance of the analogous Fe-Pt bimetallic system was found to vary significantly with respect to differing NP architectures, despite the particles' having similar elemental compositions.[11] Studies such as this highlight the importance of compositional *and* structural control of bimetallic NPs, due to their essential roles in determining the ultimate performance of a catalytic system.

Here, we present the synthesis of $CoPt_3$, CoPt, and Co_3Pt (Co_xPt_y) alloy and intermetallic NPs, which were extensively characterized by powder X-ray diffraction (XRD), transmission electron microscopy (TEM), and energy dispersive spectroscopy (EDS) analyses. We conduct a full systematic evaluation of the well-characterized Co_xPt_y NPs for CO-tolerant HOR catalysis to probe the influences of size, composition, and architecture on this energy conversion process.

2 EXPERIMENTAL

2.1 Reagents and Materials

Cobalt acetylacetonate ($Co(acac)_3$, 99.99%), platinum acetylacetonate ($Pt(acac)_2$, 97%), 1-octadecene (90%), sodium triethylborohydride solution ($NaBEt_3H$, 1.0 M in toluene), oleic acid (OA, 90%), and acetone (99.5%) were purchased from Aldrich. Methanol (MeOH, 99.8%) was purchased from VWR. Oleylamine (OAm, >70%) and Nafion® solution (5%) were purchased from Fluka. Isopropanol (iPrOH, 99%) was purchased from Pharmco-AAPER. Hexanes (99.9%) and sulfuric acid (H_2SO_4, 96.4%) were purchased from Fisher. Vulcan XC-72 carbon black powder (CB) was purchased from Cabot Corporation. E-TEK Pt (30% HP Pt on Vulcan XC-72) was purchased from BASF. Ultra-pure water was obtained from deionized water using a Millipore Academic Milli-Q A10 purifier system. All materials were used as received without further purification.

2.2 Synthesis of Co_xPt_y Alloy and Intermetallic Nanoparticles

In a typical synthesis, $Co(acac)_3$ and $Pt(acac)_2$ in the appropriate molar ratios (0.075 mmol total metal, Co:Pt ratios: 3:1, 1:1, 1:3), OA (50 µL), and OAm (50 µL) were mixed in 1-octadecene (5 mL) in a 50 mL round-bottom flask. The resultant mixture was degassed at 80 °C under vacuum, then placed under a flowing N_2 atmosphere and

held at 100 °C for 60 min to ensure full dissolution of the precursors. In a separate Schlenk flask, 1-octadecene (15 mL) was added and degassed at 80 °C under vacuum, placed under flowing N_2 and heated to 200 °C. At this temperature, $NaBEt_3H$ solution (3 mL, 1.0 M in toluene) was injected into the Schlenk flask, followed by the immediate injection of the Co_xPt_y precursor solution into the Schlenk flask. The reaction solution instantly turned black with the precursor injection, and the resultant mixture was returned to 200 °C. After being held at 200 °C for 60 min, the heating source was removed and the reaction was allowed to cool down to room temperature. The black colloidal solution was transferred to a 50 mL conical centrifuge tube, where a 1:1 MeOH/acetone mixture (40 mL) was added to the tube, which was sonicated in a sonication bath (FS30H, Fisher Scientific) for 10 min before centrifugation at 6000 rpm for 15 min. The supernatant was discarded and the washing procedure was repeated an additional two times. The black solid was dried overnight, before re-suspension in hexanes (20 mL).

To make carbon-supported Co_xPt_y electrocatalysts with 30 wt % total metal loading, the NP suspensions were mixed with a suitable amount of CB powder and sonicated in a sonication bath (FS30H, Fisher Scientific) for 180 min. The hexanes were evaporated in air overnight and the resultant CB-supported NPs were vacuum-dried. The dried solids were placed in a ceramic boat, which was introduced into a quartz glass tube and heated in a horizontal tube furnace (Thermolyne F21135, Thermo Scientific) under a 5% H_2/95% Ar atmosphere with a flow rate of 90 SCCM for 90 min at 400 °C, 550 °C, or 700 °C to remove the surfactants from the NPs (400 °C, 550 °C, 700 °C) and/or convert the alloy particles into their intermetallic counterparts (550 °C and 700 °C).

2.3 Characterization Methods

Powder X-ray diffraction (XRD) patterns of samples were obtained on a Bruker C2 Discover diffractometer equipped with a VÅNTEC-500 detector using a monochromatic Cu Kα radiation source biased at 40 kV and 40 mA. Transmission electron microscope (TEM) images were obtained on a JEM 2100F Field Emission TEM operating at 200 kV. Energy dispersive spectroscopy (EDS) data were collected on the same TEM operating in the scanning (STEM) mode.

2.4 Electrochemical Analysis

iPrOH (159.2 mL), ultra-pure water (40.0 mL), and Nafion® solution (0.80 mL, 5%) were mixed and stored as a stock solution. The catalyst ink was prepared by mixing the supported NP powder with the above stock solution such that the concentration was 1.0 mg/mL of powder in solution. The resultant mixture was sonicated in a sonication bath (FS30H, Fisher Scientific) for 120 min. The catalyst ink (20 μL) was cast on a glassy carbon (GC) electrode (Pine Instruments, 5.0 mm diameter) using a micropipette and allowed to dry in air overnight while covered. Electrochemical experiments were performed on a potentiostat (Autolab PGSTAT30) with a standard three-electrode electrochemical cell. The rotating GC disk electrode with dried catalyst ink on its surface was used as the working electrode. Pt wire was used as the counter electrode and a saturated calomel electrode (SCE) was used as the reference electrode. All potentials were recorded with respect to the SCE. H_2SO_4 in ultra-pure water (0.5 M) was used as the electrolyte. The catalysts were subjected to 50 potential scan cycles at 50 mV/s between -0.2 V and 0.8 V while Ar-saturated as a conditioning procedure. After catalyst conditioning, fresh electrolyte was used during the collection of experimental data. To perform the CO stripping experiment, the catalyst was saturated with CO by bubbling CO (99.5% pure, Al tank) in the electrolyte for 20 min, followed by Ar-purging for 40 min to remove excess CO. The CO-saturated catalysts were then subjected to a potential scan cycle at 20 mV/s between -0.2 V and 0.8 V. To obtain polarization curves for the electrooxidation of CO-contaminated H_2, the electrolyte was bubbled with a 1000 ppm CO/balance H_2 gas mixture (99% pure, Al tank) for 90 min with the electrode potential held at -0.2 V, followed by a potential scan (1 mV/s) at a rotation rate of 1600 rpm.

3 RESULTS AND DISCUSSION

3.1 Synthesis and Characterization of Co_xPt_y Nanoparticles

Briefly, bimetallic Co_xPt_y ($CoPt_3$, CoPt, and Co_3Pt) NPs were synthesized by using $NaBEt_3H$ to co-reduce appropriate amounts of $Co(acac)_3$ and $Pt(acac)_2$ in 1-octadecene in the presence of an OA/OAm surfactant mixture at 200 °C similarly to previously reported methods.[12,13] The three different as prepared (AP) Co_xPt_y samples ($CoPt_3$, CoPt, and Co_3Pt) were annealed at three different temperatures (400 °C, 550 °C, and 700 °C) to convert the disordered alloys into ordered intermetallic phases. The results of our experiments are in good agreement with previous reports.[12,13] A summary of the experimental data, as determined from XRD, TEM, and EDS analyses of the NPs, is shown in Table 1.

Representative XRD patterns of the Co_xPt_y NPs are shown in Figure 1. Relative to monometallic Pt, the diffraction peaks shift to increasingly higher 2θ angles with increasing Co concentration due to increasing lattice contraction resulting from Co having a smaller lattice constant than Pt. Each of the Co_xPt_y NPs samples also were analyzed with EDS (graphical data not shown for brevity), with the $CoPt_3$, CoPt, and Co_3Pt NPs having average Co:Pt composition ratios of 24:76, 45:55, and 70:30, respectively, in good agreement with the precursor ratios used and the XRD analysis. The composition ratios do not change significantly with respect to annealing temperature.

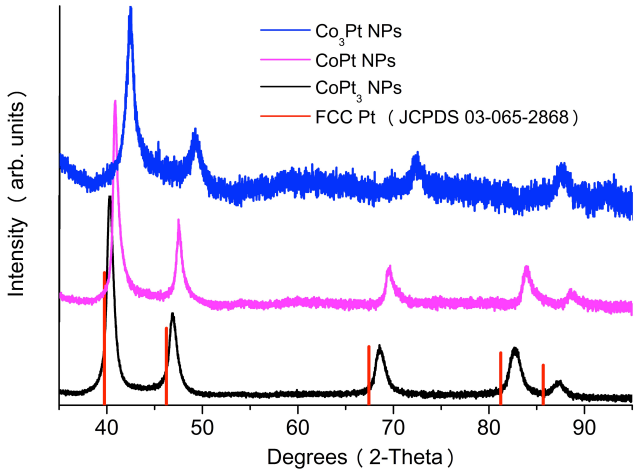

Figure 1. XRD patterns of 550 °C annealed $CoPt_3$ (black), CoPt (magenta), and Co_3Pt (blue) NPs. Red lines indicate the peak positions for FCC phase Pt.

Comparing the different Co_xPt_y NPs shows that the particles generally increase in size with increasing Pt content (Table 1). Each Co_xPt_y synthesis contained the same amount of surfactant with equal moles of total metal, with only the Co:Pt ratios changing between the different Co_xPt_y syntheses. Increasing the Pt content (but maintaining equal moles of metal) within a synthesis results in slightly increased surface area due to the larger size of Pt atoms relative to Co. Since surfactants control NP size with respect to surface area, the increased surface area effectively increases the metal-surfactant ratio, which leads to a slight increase in NP size.

While the Co-Pt phase diagram shows that the $CoPt_3$ and CoPt NPs should exist as intermetallics, the rapid reduction and nucleation of Co and Pt results in the formation of Co_xPt_y alloy particles. Annealing the $CoPt_3$ and CoPt NPs induces their transformation into their thermodynamically stable intermetallic phases, while the Co_3Pt NPs maintain the expected alloy structure. High temperature annealing is necessary to induce the transformation from alloy to intermetallic, but it also results in the growth and agglomeration of the NPs (Table 1). A representative TEM image of the Co_xPt_y NPs is shown in Figure 2.

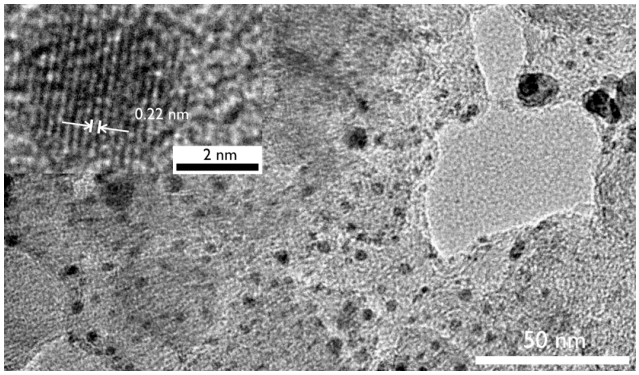

Figure 2: Representative TEM image of Co_xPt_y NPs (550 °C annealed CoPt NPs shown)

3.2 Electrochemical Characterization of Co_xPt_y Alloy and Intermetallic Nanoparticles

To assess the effects of size, composition and architecture on the NPs' catalytic activities, we evaluated the catalytic activities of all nine annealed (400 °C, 550 °C, and 700 °C) Co_xPt_y catalysts for CO oxidation (CO stripping) and CO-tolerant HOR. As a reference, the commercially available E-TEK Pt catalyst was tested under identical conditions. All catalysts were prepared with a 30% total metal loading by weight based on the initial amounts of reagents. Given the similar metal loadings of the Co_xPt_y NP catalysts, we focus our analysis on how the different sizes, compositions and architectures of the NPs impact their resultant catalytic activities. Enhanced catalytic activity is associated with *lower* onset potential (E_{Onset}) values. A summary of the relevant structural and electrochemical data for the different NP catalysts is given in Table 1.

The onset potentials for CO oxidation on the Co_xPt_y catalysts are all in the range of 0.4 - 0.55 V (Table 1), which is similar to the 0.53 V onset potential for the E-TEK Pt reference. Comparing the composition sets ($CoPt_3$ vs. CoPt vs. Co_3Pt), reveals that the onset potential tends to decrease with increasing Co content. Previous studies have demonstrated that the electronic structure modifications induced by alloying Pt catalysts with Co improves their ability to oxidize CO in the absence of H_2.[14,15] The results of these previous CO stripping experiments are reproduced here.

For the electrooxidation of CO/H_2 mixtures (1000 ppm CO), the onset potentials range from 0.27 - 0.4 V, which is lower than the pure CO oxidation onset potentials as expected (Table 1). The $CoPt_3$-400 °C and all three Co_3Pt catalysts have CO/H_2 onset potentials very similar to E-TEK Pt, while the 550 °C and 700 °C annealed CoPt and $CoPt_3$ catalysts have much lower CO tolerances. Unlike other studies where lower CO stripping onset potentials are correlated with lower CO/H_2 onset potentials and increased CO tolerance, there is no clear correlation between the CO oxidation and onset potentials in the Co_xPt_y catalysts.[16]

This lack of correlation suggests the diminished CO tolerance in the intermetallic NPs is most likely due to modified electronic structures that negatively impact their ability to tolerate CO relative to the alloy particles. As previously seen in $FePt_3$ catalysts, this loss of CO tolerance would most likely manifest through reduced H_2 adsorption and activity for HOR.[11] This explanation would also account for the CO tolerance of the CoPt-400 °C catalyst, which is of mixed alloy/intermetallic state and behaves intermediate of the two architectures.

Table 1. Summary of representative experimental data for NPs

Sample	Space Group (Crystal Structure)[a]	Avg. NP Size[b]	Avg. NP Composition[c]	CO Stripping E_{Onset}[d]	CO/H_2 Oxidation E_{Onset}[d]
E-TEK Pt	Fm-3m (FCC)	3.2 ± 0.8 nm	--	0.53	0.29
$CoPt_3$-400 °C	Fm-3m (FCC)	2.8 ± 1.3 nm	Co:Pt 24:76	0.50	0.29
$CoPt_3$-550 °C	Pm-3m (Primitive)	6.0 ± 3.8 nm		0.47	0.38
$CoPt_3$-700 °C	Pm-3m (Primitive)	6.9 ± 4.0 nm		0.54	0.40
CoPt-400 °C	Fm-3m (FCC) P4/mmm (FCT)	2.7 ± 0.7 nm	Co:Pt 45:55	0.48	0.34
CoPt-550 °C	P4/mmm (FCT)	4.7 ± 3.2 nm		0.45	0.37
CoPt-700 °C	P4/mmm (FCT)	6.0 ± 3.9 nm		0.45	0.39
Co_3Pt-400 °C	Fm-3m (FCC)	2.2 ± 0.6 nm	Co:Pt 70:30	0.47	0.29
Co_3Pt-550 °C	Fm-3m (FCC)	3.9 ± 2.5 nm		0.42	0.31
Co_3Pt-700 °C	Fm-3m (FCC)	4.9 ± 3.9 nm		0.41	0.27

[a] Determined from XRD analysis. [b] Calculated by counting 100 small particles and agglomerates.
[c] Determined from EDS analysis. [d] Potential vs. SCE.

4 CONCLUSION

In summary, a series of Co_xPt_y NPs with controlled compositions and architectures were synthesized through a simple co-reduction method. The Co_xPt_y electrocatalysts were tested for their activities towards CO-tolerant HOR to probe the influences of size, composition, and architecture. The Co_xPt_y catalysts were found to have similar or less CO tolerance relative to monometallic Pt, with the structural and electronic modifications induced by the atomic ordering of Co and Pt found to negatively impact their activity for the HOR. Overall, the Co_3Pt NPs have HOR catalytic activities comparable to monometallic Pt, but utilize far less Pt to achieve this result, leading to a significant reduction in the overall cost of the electrocatalyst.

5 ACKNOWLEDGEMENTS

We thank the Air Force Office of Scientific Research for financial support of this work through AFOSR grant FA9550-09-1-0523 and AFOSR grant 4789-UM-AFOSR-0004. C. S. acknowledges the support of the Ann G. Wylie Dissertation Fellowship. We also acknowledge the support of the Maryland NanoCenter and its NispLab. The NispLab is supported in part by the National Science Foundation as a MRSEC Shared Experimental Facility.

REFERENCES

[1] E. Antolini, J.R.C. Salgado, E.R. Gonzalez, J. Power Sources 160 (2006) 957.
[2] M. Oezaslan, P. Strasser, J. Power Sources (2011).
[3] N.M. Marković, T.J. Schmidt, V. Stamenkovic, P.N. Ross, Fuel Cells 1 (2001) 105.
[4] J. Greeley, I.E.L. Stephens, A.S. Bondarenko, T.P. Johansson, H.A. Hansen, T.F. Jaramillo, J. Rossmeisl, I. Chorkendorff, J.K. Nørskov, Nat. Chem. 1 (2009) 552.
[5] V.R. Stamenkovic, B.S. Mun, M. Arenz, K.J.J. Mayrhofer, C.A. Lucas, G. Wang, P.N. Ross, N.M. Markovic, Nat. Mater. 6 (2007) 241.
[6] Q. He, S. Mukerjee, Electrochim. Acta 55 (2010) 1709.
[7] S. Koh, M.F. Toney, P. Strasser, Electrochim. Acta 52 (2007) 2765.
[8] D. Wang, H.L. Xin, R. Hovden, H. Wang, Y. Yu, D.A. Muller, F.J. DiSalvo, H.D. Abruna, Nat. Mater. 12 (2012) 81.
[9] S.K. Cheah, O. Sicardy, M. Marinova, L. Guetaz, O. Lemaire, P. Gélin, A.A. Franco, J. Electrochem. Soc. 158 (2011) B1358.
[10] S.M.M. Ehteshami, Q. Jia, A. Halder, S.H. Chan, S. Mukerjee, Electrochim. Acta 107 (2013) 155.
[11] Z. Liu, G.S. Jackson, B.W. Eichhorn, Energy Environ. Sci. 4 (2011) 1900.
[12] E. Favry, D. Wang, D. Fantauzzi, J. Anton, D.S. Su, T. Jacob, N. Alonso-Vante, Phys. Chem. Chem. Phys. 13 (2011) 9201.
[13] E.V. Shevchenko, D.V. Talapin, H. Schnablegger, A. Kornowski, Ö. Festin, P. Svedlindh, M. Haase, H. Weller, J. Am. Chem. Soc. 125 (2003) 9090.
[14] H. Igarashi, T. Fujino, Y. Zhu, H. Uchida, M. Watanabe, Phys. Chem. Chem. Phys. 3 (2001) 306.
[15] C. Xu, J. Hou, X. Pang, X. Li, M. Zhu, B. Tang, Int. J. Hydrogen Energ. 37 (2012) 10489.
[16] Z. Liu, J.E. Hu, Q. Wang, K. Gaskell, A.I. Frenkel, G.S. Jackson, B. Eichhorn, J. Am. Chem. Soc. 131 (2009) 6924.